Available online at www.elixirpublishers.com (Elixir International Journal)

Nanotechnology

Elixir Nanotechnology 99 (2016) 43293-43299

ISSN: 2229-712X

Quantum Chemical, DFT and Electron Density Studies on Nano-Organic Semiconductor for Field Effect Transistors (OFETs): 2-phenyl-*3H*pyrrole Molecule

V.S. Lakshmepriyaa[1]*,Joe. G. Jesudurai[1] and K. Selvaraju[2]
[1]Department of Physics, Loyola college, Chennai- 600 034, India.
[2]Department of Physics, Kandaswami Kandar's College, Velur-638 182, Namakkal., India.

ARTICLE INFO

Article history:
Received: 9 September 2016;
Received in revised form:
19 October 2016;
Accepted: 26 October 2016;

Keywords
DFT,
Charge density,
Energy gap,
Atomic Charges,
Electrostatic Potential.

ABSTRACT

The electron density and charge transport studies of organic field effect transistors (OFETs) based 2-phenyl-*3H*pyrrole molecule have been calculated from the quantum chemical and DFT methods. Density functional theory calculations with B3LYP/aug-cc-PVDZ basis sets was used to determine ground state gas space molecular geometries (bond lengths and bond angles), electron density and bonding features of this molecule. The electron densities at the bond critical point (BCP) of aromatic Car–Car bonds are much stronger than the other bonds in the molecule. The calculated HOMO and LUMO energies is ~5.50 eV [B3LYP/aug-cc-PVDZ], this shows that charge transfer occurs within the molecule. The HOMO–LUMO gap calculated from quantum chemical calculations has been compared with the value calculated from the density of states. The negative electrostatic potential (ESP) is concentrated solely around the N atoms, whereas in the rest of the region a positive ESP to dominate.

Introduction

Nowadays organic semiconductors (OSCs) have been explored extensively in optoelectronic applications, such as organic light emitting diodes (OLEDs) [1,2], organic field-effect transistors (OFETs) [3-5], and organic solar cells [6,7]. Development of high-performance organic semiconductors [8,9] plays a crucial role in the fabrication of high-resolution, full-color, and flat-panel displays [10,11]. The advantage of the organic semiconductors over the conventional inorganic semiconductor materials such as silicon and germanium is ultralow cost, light weight, and flexibility. Since, organic field-effect transistors (OFETs) have attracted increasing research interest due to their potential applications in the field of flexible displays, integrated circuits, low-cost electronic devices and gas sensor [12]. In addition to the π conjugated organic oligomers and polymers as a considerable research subject in OFETs field [13]. Recent years, synthetic aspects of the OFETs investigation have been largely on a trial and error basis, mostly depending on empirical rules, such as the prediction of wavelengths based on HOMO and LUMO energy levels. If the relationship between the optoelectronic properties and molecular structures of OFETs is systematically understood, designing of these materials would be more facile and economical. However, design and synthesis of such organic materials with satisfactory multifunctional properties for high-performance OFETs remain challenging [14].

Theoretical understanding of their structural parameters, conductivity and electronic excitations is significantly important in computer-aided design and optimization of the OFETs molecule like electroluminescent oligomers and polymers.Quantum chemical investigations that have tremendously affected synthetic chemistry through studies of structure property relationship and underlying mechanism seem to have been much less helpful for studying OFETs materials in this respect, probably due to the large size of molecules [15]. Recent progress in quantum chemical methods, especially the advent of density functional theory (DFT) and charge density analysis, now allows systematic calculations for the structure and properties of OFETs materials both in electronically ground and excited states to provide invaluable knowledge for photo absorption and emission, and charge carrier mobility [16,17].

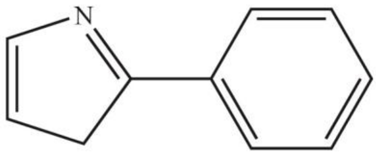

Figure 1. Chemical Structure of 2-phenyl-*3H*pyrrole.

The Pyrrole based conjugated materials (oligothiophenes and polythiophenes) are among the most promising materials for OFETs and other electronic devices based on organic semiconductors [18]. In this context, 2-phenyl-*3H*pyrrole (Figure.1) has been incorporated into oligomers and polymers more recently. In 2008, phenyl-*3H*pyrrole and thiophene moieties were reported; OFET hole mobilities up to 0.21 cm^2/Vs suggest the moiety is a promising building block for hole-transport materials [19]. Hence, to understand the molecular geometric and transport properties of 2-phenyl-*3H*pyrrole based OFETs, the above properties are essential. The main aims of the present study are to (i) predict the conformation of the above structure (ii) determine the charge

Tele:
E-mail address: vslakshmepriyaa@gmail.com

transport mechanisms (ground state) from quantum chemical calculations, and (iii) estimate other possible electrical properties by computational methods.

The topological properties of the bonds such as electron density, its gradient vector field $\nabla\rho(r)$ and its Laplacian $\nabla^2\rho_{bcp}(r)$ reveal the nature of the bonds between the atoms in molecules (AIM) [20,21]. The pairs of gradient lines in the $\nabla\rho(r)$ field originated at the saddle critical point between atoms and terminated at two neighbouring nuclei along which the electron density is maximal with respect to any other line are the most important for characterization of the atomic interactions. They form the atomic interaction lines namely the bond path in an equilibrium system corresponding bond critical points (BCP) are denoted as (3, -1); they are characterized by three non-zero eigen values of the curvature or Hessian matrix λ_i and the sum of the algebraic signs of λ_i is -1, values $\lambda_1 < 0$ and $\lambda_2 < 0$ measure the degree of the electron density contraction towards the BCP, while $\lambda_3 > 0$ measures the degree of the ED contraction towards each of the bonded nuclei, signs of the Laplacian at the bond critical point $\nabla^2\rho_{bcp}(r)$ depends on the relationship between the λ_i values at this point.

Computational Details

To obtain the exact geometry and the electronic parameters of the 2-phenyl-*3H*pyrrole molecule, a minimum energy structure optimization is carried out from the HF and B3LYP level of theories with the basis sets 6-311G** [22] and aug-cc-PVDZ [23] using Gaussian03 program [24]. The optimizations converged at the threshold values for HF (Maximum Force: 0.000034 au, 0.000005 au, root mean square (RMS) force: 0.001153 au, 0.000250 au) and Density Functional Theory (DFT) (Maximum force: 0.000011 au, 0.000048 au, RMS force: 0.000003 au, 0.000074 au) methods, respectively. The wave function obtained from the optimization is used to calculate the bond topological properties such as bond electron density, Laplacian of electron density and bond ellipticity at the BCPs using the Bader's theory of AIM implemented in AIMPAC software [25]. The atomic charges are calculated from the AIMALL [26] software package. The deformation densities of the molecule have been plotted using the software wfn2plots and XD package [27]. The 3D plot software [28] is used to generate the Electrostatic potential (ESP**)** map of the molecule.

Results and discussion

Structural aspects and dipole moment

Figure 2 shows the ball and stick model of energy minimized geometry of 2-phenyl-*3H*pyrrole molecule. The structural parameters of the molecule such as bond lengths, bond angles, and torsion angles were calculated from the HF/6-311G**, B3LYP/6-311G** and B3LYP/aug-cc-PVDZ level calculations. Careful examination of the geometrical parameters, specifically, the bond distances predicted by HF method are found to be consistently shorter than the DFT methods. In benzene ring, the C–C bond lengths calculated from HF method are ranged from 1.383 to 1.390 Å and the average value is 1.386 Å. In pyyrole ring, the C–C bond distances are not equal, and its average value is 1.520 Å. The DFT method predicts the distances for the above rings that ranged from 1.513 to 1.560 Å and the average value is 1.536 Å , which is slightly longer than the C–C distance predicted by HF and the difference is 0.026 Å. Notably, the correlation effect in DFT found slightly longer distances for the C(7)–C(11) and C(10)–C(11) (1.548 and 1.534 Å) bonds distances, as it was found almost equal for all C–C bonds in HF calculations. Notably, the average C–C bond length of pyrrole ring and the ranges from 1.446 to 1.540 Å, which, is almost equal to the C–C bond length of the reported molecule [29]. The C–N bond length of pyrrole ring is 1.482 Å [B3LYP/agu-cc-PVDZ], respectively.

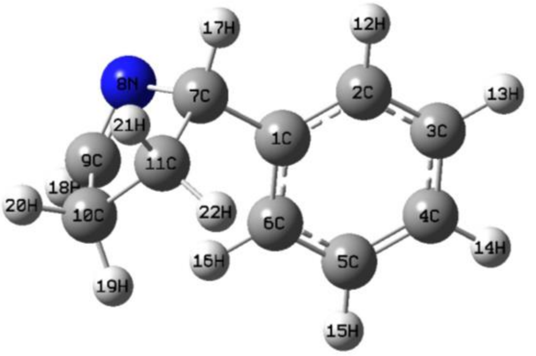

Figure 2. The atom numbering scheme of 2-phenyl-*3H*pyrrole B3LYP/aug-cc-PVDZ level.

Further, this distance is longer than the distance [1.371 Å] reported by theoretical study [29]. The C–C–C bond angles of benzene ring predicted by HF/6-311G** and DFT methods (Table.1) are found to be almost equal and the average value is 120°. The torsion angle of C(1)–C(7)–N(8)–N(9) and C(11)–C(7)–N(8)–N(9) bonds is 81.4 and -35.4°; this wide angle twist indicates that, the pyrrole group in the molecule exhibit *trans* conformation with respect to benzene ring and this angle is almost equal to the theoretical structure [18].

The dipole moment (μ) of 2-phenyl-3Hpyrrole molecule is calculated form B3LYP/aug-cc-PVDZ level theory. When the molecules enter into the electric field the dipole moments of the molecules may significantly altered and the orientation of the dipole moment vectors. In the gas phase dipole moments of above molecules is ~2.20 D respectively, these values are may abruptly increased when molecule undergoes electric fields.

Electron density analysis

Figure 3 shows the deformation density plots of 2-phenyl-*3H*pyrrole OFETs based molecule. The deformation density shows the non-spherical nature of the electron density of atoms in the molecule due to bond formation. The theory of Atoms in Molecules (AIM) developed by R.F.W. Bader and his co-workers can be implemented to analyze the charge density distribution and electrostatic properties of molecules from quantum chemical theory. The theory allows predicting the precise energetic nature of the bond, and it can easily relate to bond density, Laplacian of electron density [$\nabla^2\rho_{bcp}(r)$] at BCP [20]. The critical point search has been carried out for all bonds of the molecule, as a result, invariably found a (3, -1) critical point in all homo and hetro atomic bonds.

The structure of the molecule can be stated as two rings connected with a C–C bond at the centre. The HF method predicted the bond density $\rho_{bcp}(r)$ at the critical points of C–C bonds of benzene ring that ranged from 2.18 to 2.20 eÅ^{-3} and the average value is 2.19 eÅ^{-3}[Table.2], whereas the DFT methods predicts slightly lower level densities and the average value is 2.07 [B3LYP/6-311G** and 2.05 [B3LYP/aug-cc-PVDZ] eÅ^{-3}; this value is found well close to the reported experimental densities of similar type of ring structures.

Table 1. Geometric parameters of 2-phenyl-*3H*pyrrole molecule (Å, °).

Bond Lengths (Å)	**HF/6-311G****	**B3LYP/6-311G****	**B3LYP/aug-cc-PVDZ**
C(1)–C(2)	1.390	1.399	1.403
C(1)–C(6)	1.387	1.397	1.402
C(2)–C(3)	1.383	1.392	1.398
C(3)–C(4)	1.385	1.394	1.398
C(4)–C(5)	1.383	1.393	1.399
C(5)–C(6)	1.386	1.394	1.398
C(1)–C(7)	1.515	1.515	1.515
C(7)–N(8)	1.465	1.480	1.482
C(7)–C(11)	1.548	1.560	1.560
N(8)–C(9)	1.250	1.270	1.276
C(9)–C(10)	1.510	1.513	1.514
C(10)–C(11)	1.534	1.541	1.543
C(2)–H(12)	1.077	1.086	1.092
C(3)–H(13)	1.076	1.085	1.091
C(4)–H(14)	1.076	1.084	1.091
C(5)–H(15)	1.076	1.085	1.091
C(6)–H(16)	1.073	1.083	1.089
C(9)–H(18)	1.080	1.089	1.095
C(7)–H(17)	1.088	1.098	1.103
C(10)–H(19)	1.085	1.093	1.099
C(10)–H(20)	1.089	1.098	1.103
C(11)–H(21)	1.083	1.091	1.096
C(11)–H(22)	1.085	1.093	1.098
Bond Angle (°)			
C(2)–C(1)–C(6)	118.6	118.7	118.7
C(2)–C(1)–C(7)	119.4	119.7	119.8
C(6)–C(1)–C(7)	122.0	121.6	121.5
C(1)–C(2)–C(3)	120.9	120.8	120.9
C(2)–C(3)–C(4)	120.1	120.1	120.0
C(3)–C(4)–C(5)	119.4	119.5	119.5
C(4)–C(5)–C(6)	120.5	120.4	120.3
C(1)–C(6)–C(5)	120.5	120.5	120.6
C(1)–C(7)–N(8)	113.3	113.2	113.2
C(1)–C(7)–C(11)	114.1	114.1	114.1
N(8)–C(7)–C(11)	105.3	105.6	105.8
N(8)–C(7)–H(17)	106.5	106.0	106.0
C(7)–N(8)–C(9)	109.4	108.8	108.9
N(8)–C(9)–C(10)	116.4	116.7	116.5
C(9)–C(10)–C(11)	100.5	100.9	101.1
C(7)–C(11)–C(10)	102.8	103.1	103.3
Torsion Angle (°)			
C(6)–C(1)–C(2)–C(3)	-0.6	-0.6	-0.5
C(7)–C(1)–C(2)–C(3)	177.9	177.9	177.3
C(2)–C(1)–C(6)–C(5)	0.5	0.5	0.3
C(7)–C(1)–C(6)–C(5)	-178	-178	-177.5
C(2)–C(1)–C(7)–N(8)	161.2	163.4	152.4
C(2)–C(1)–C(7)–C(11)	-78.3	-75.7	-86.6
C(6)–C(1)–C(7)–N(8)	-20.4	-18.2	-29.9
C(6)–C(1)–C(7)–C(11)	100.1	102.7	91.2
C(1)–C(2)–C(3)–C(4)	0.3	0.3	0.4
C(2)–C(3)–C(4)–C(5)	0.1	0.2	0.1
C(2)–C(3)–C(4)–H(14)	179.7	179.8	179.6
C(3)–C(4)–C(5)–C(6)	-0.2	-0.3	-0.3
C(4)–C(5)–C(6)–C(1)	-0.1	0	0.1
C(1)–C(7)–N(8)–C(9)	140.9	140	139.5
C(11)–C(7)–N(8)–C(9)	15.6	14.4	13.9
N(8)–C(7)–C(11)–C(10)	-23	-21.5	-20.5
C(7)–N(8)–C(9)–C(10)	-1	-0.7	-0.9
N(8)–C(9)–C(10)–C(11)	-13.8	-13.2	-12.4
C(9)–C(10)–C(11)–C(7)	21.1	19.9	18.9

The HF method, the C(7)–N(8) and C(9)–N(8) bond density found 1.863 and 2.733 eÅ^{-3}, notably, the HF method and the same found difference found in the DFT methods and the values are ~1.760 and 2.62 eÅ^{-3} respectively.

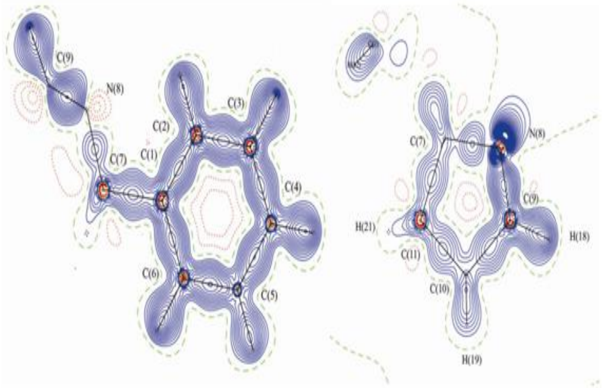

Figure 3. Deformation density maps of 2-phenyl-*3H*pyrrole molecule. Solid lines represent positive contours, dotted lines are negative contours and dashed lines are zero contours. The contours are drawn at 0.05 e Å^{-3} interval.

Interestingly, the large difference of density exist between HF method and DFT methods; this marginal variation is due to the electron correlation and basis set effects [Table.2]. For the case of electron density at BCP for C–H bonds ranges from ~1.91 eÅ^{-3}to 1.93 eÅ^{-3}, can also states that approximately equal electron density throughout C–H bonds. The predicted value stands equal with the experimental values [29]. Studies were made to position the location of bcp for each bond. From the studies it was found that the bcp were located almost centre, or equally distant from each carbon atoms in every C–C bonds and also for C–N bond, BCP found to be at exact centre of the bond [Figure .4].

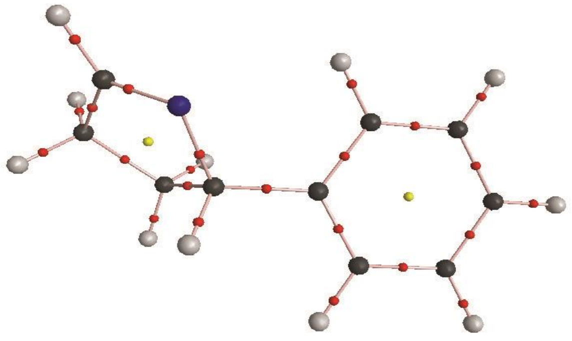

Figure 4. The molecular graph showing the (3, -1) and (3,+1) critical points of the 2-phenyl-*3H*pyrrole molecule.

The bond path analysis has been carried out to understand the bond charge polarization of each bond in the molecule; in which the Car–Car bonds are the less polarized bonds, which is confirmed from the small bcp shift of about less than 0.9%. But, the trend in the C–N bonds are found significantly different, i.e., the bcp positions of these bonds are shifted largely from the middle of the bonds at about 13%, towards the respective carbon atoms; this amount of shift indicates that the charges of these bonds are highly polarized. Table 3, shows the complete spectrum of bond charge polarization of the molecule, in which, the C–N and N–H bonds are considered as the highly polarized bonds.

The bond ellipticity [24,25], ε = (λ_1/λ_2-1) is defined as the measure of anisotropy of electron distribution at BCP, where λ_1 and λ_2 are the negative eigen values of Hessian matrix [24]. The high ellipticity value indicates the large anisotropy of bonding density ρ_{bcp} and hence a strong deviation from σ-type bond character [24]. The ellipticity of C–C bonds of rings are found small and the value ranges 0.05–0.20 (Table.2), indicates, that the bond densities are highly isotropic. Both methods predicted a large ε -values for C–N bonds five membered ring, shows, the densities are highly anisotropic, and the trend is same in C–N bonds.

Molecular Orbitals and Density of States

The chemical oxidation of phenyl rings will affect the frontier orbitals, especially for HOMOs and LUMOs, which are closely related to gain and loss electrons during the charge transport [30]. The energy gap between HOMO and LUMO and the relative orderings of HOMO and LUMO levels will be modulated as well [31]. The HOMO and LUMO are distributed all over the molecules because the molecular planarity and extended π conjugation. The energy gap between the HOMO and LUMO molecular orbitals is a critical parameter in determining molecular electrical transport properties because it is a measure of electron conductivity. The highest occupied molecular orbitals are localized mainly on the benzene ring system. The calculated frontier orbital energies HOMO and LUMO and energy gaps between highest occupied molecular orbitals (HOMO) and lowest unoccupied molecular orbitals (LUMO) are shown in Figure 6. The computed energy values of HOMO and LUMO in gas phase are 12.08 eV [HF/6-311G**]; 5.57 eV [B3LYP/6-311G**] and 5.50 eV [B3LYP/aug-cc-PVDZ] respectively. The energy gap between HOMO and LUMO determines the kinetic stability, chemical reactivity and, optical polarizability and chemical hardness–softness of a molecule [31].

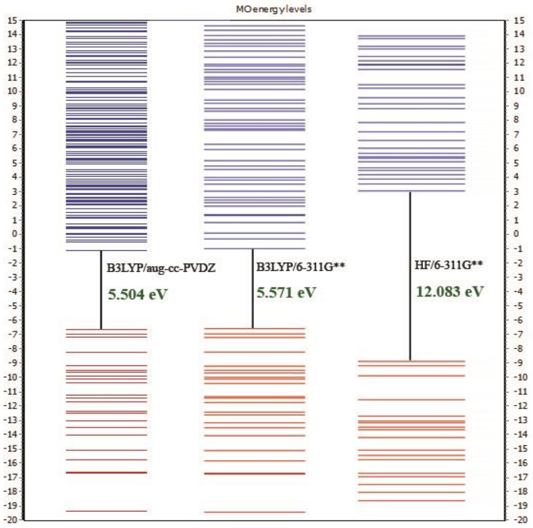

Figure 5. Molecular orbital energy level for B3LYP/aug-cc-PVDZ calculations.

The HLG decreases from 12.08 to 5.504 eV. This variation is also confirmed from the spectrum of density of states (DOS). Figures 7(a)-(c) show the DOS of 2-phenyl-*3H*pyrrole molecule with different levels, notably, the lower level broadens the DOS peaks. Seemingly, the significant decrease of HLG may facilitate large electron conduction [32] through the molecule.

Table 2. Bond topological properties 2-phenyl-*3H*pyrrole molecule. [First line: HF/6-311G, Second line: B3LYP/6-311G** and Third line:B3LYP/aug-cc-PVDZ].**

Bonds	$\rho_{bcp}(r)$[a]	ε[b]	d_1[c]	d_2[c]	D[c]
C(7)–C(1)	1.792	0.053	0.749	0.766	1.515
	1.703	0.051	0.756	0.759	1.515
	1.706	0.041	0.754	0.761	1.515
C(1)–C(2)	2.176	0.239	0.697	0.693	1.391
	2.069	0.206	0.702	0.698	1.399
	2.048	0.200	0.702	0.701	1.403
C(2)–C(3)	2.197	0.241	0.692	0.691	1.383
	2.091	0.208	0.697	0.695	1.392
	2.06	0.200	0.700	0.698	1.398
C(6)–C(1)	2.183	0.238	0.684	0.704	1.387
	2.076	0.204	0.692	0.705	1.397
	2.048	0.194	0.697	0.705	1.402
C(4)–C(3)	2.192	0.233	0.689	0.696	1.385
	2.086	0.201	0.695	0.699	1.394
	2.059	0.197	0.698	0.700	1.398
C(5)–C(4)	2.200	0.237	0.693	0.691	1.383
	2.092	0.203	0.696	0.696	1.393
	2.060	0.197	0.699	0.699	1.399
C(6)–C(5)	2.188	0.230	0.690	0.697	1.386
	2.086	0.198	0.695	0.698	1.394
	2.059	0.195	0.698	0.700	1.398
N(8)–C(7)	1.863	0.022	0.917	0.549	1.466
	1.770	0.010	0.856	0.625	1.480
	1.757	0.008	0.866	0.617	1.483
C(9)–N(8)	2.733	0.230	0.423	0.828	1.251
	2.623	0.220	0.454	0.817	1.271
	2.613	0.183	0.434	0.843	1.277
C(9)–C(10)	1.798	0.040	0.779	0.732	1.510
	1.828	0.009	0.387	0.697	1.084
	1.695	0.041	0.772	0.743	1.514
C(11)–C(7)	1.685	0.015	0.769	0.780	1.548
	1.701	0.042	0.769	0.744	1.513
	1.564	0.011	0.776	0.784	1.560
C(10)–C(11)	1.697	0.009	0.777	0.757	1.534
	1.596	0.007	0.776	0.764	1.541
	1.592	0.012	0.778	0.765	1.543
C(3)–H(13)	1.977	0.018	0.680	0.38	1.059
	1.899	0.017	0.692	0.378	1.07
	1.877	0.014	0.691	0.372	1.062
C(4)–H(14)	1.976	0.02	0.679	0.38	1.059
	1.899	0.019	0.691	0.378	1.070
	1.877	0.015	0.690	0.372	1.062
H(15)–C(5)	1.978	0.017	0.379	0.68	1.059
	1.900	0.017	0.378	0.692	1.070
	1.877	0.013	0.372	0.691	1.063
H(20)–C(10)	1.904	0.009	0.392	0.681	1.073
	1.562	0.014	0.776	0.784	1.560
	1.811	0.009	0.388	0.688	1.076
H(16)–C(6)	1.999	0.020	0.371	0.685	1.057
	1.917	0.018	0.371	0.697	1.068
	1.890	0.013	0.366	0.695	1.061
C(2)–H(12)	1.966	0.021	0.678	0.383	1.061
	1.889	0.02	0.691	0.381	1.072
	1.869	0.015	0.688	0.376	1.064
C(7)–H(17)	1.960	0.021	0.685	0.387	1.072
	1.869	0.018	0.701	0.383	1.084
	1.854	0.021	0.691	0.385	1.076
H(18)–C(9)	1.992	0.014	0.374	0.689	1.064
	1.904	0.015	0.374	0.701	1.075
	1.886	0.016	0.367	0.700	1.066
H(19)–C(10)	1.927	0.010	0.389	0.680	1.069
	1.853	0.010	0.384	0.695	1.079
	1.834	0.009	0.384	0.687	1.072
C(11)–H(21)	1.935	0.004	0.677	0.391	1.068
	1.868	0.004	0.693	0.384	1.077
	1.849	0.003	0.685	0.384	1.069
H(22)–C(11)	1.943	0.008	0.389	0.680	1.069
	1.872	0.009	0.383	0.696	1.079
	1.854	0.007	0.384	0.687	1.071

[a] The electron density qbcp(eÅ^{-3})

[b] ε, is the ellipticity,

[c] d_1 and d_2 are the distances in Å, between CP and respective atoms of bonds.

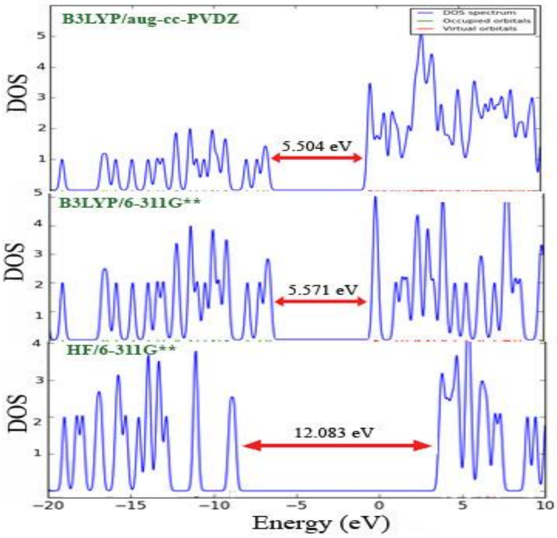

Figure 6. Shows the density of states (DOS) of 2-phenyl-*3H*pyrrole molecule with different level of theory.

Atomic Charges and Electrostatic potential

The knowledge of charge distribution of the molecule is very much essential to understand the chemical reactivity, molecular electrostatic potential and the electrostatic interactions [33]. To explore the ESP of the molecule, here, we report two kinds of charges, which are obtained from Mulliken population analysis (MPA) [34], Natural Population Analysis (NPA) [35]. The MPA and NPA charges are calculated from the method given in, which are implemented in Gaussian03 software [24]. The charges calculated from these methods are presented in Table 3. Relatively, the MPA charges are consistently higher than the NPA models charges.

The MPA charges of C(5), C(7) and C(8) are found positive and the values are 0.07 e, 0.375 e and 0.360 e, whereas the corresponding NPA charges is found negative (-0.220 e, -0.077 e); the difference between these two model charges are may be due to different method of atomic charge estimation in the molecule. In the other hand, all other C-atoms have found negative charges. The average charge of N-atoms is found high negative and the value is -0.567 e (MPA) and -0.482 e (NPA). The difference of charge between C and N atoms of this molecule implies that these bonds are highly polarized; presumably, the bond charge polarization partly weakening the bond.

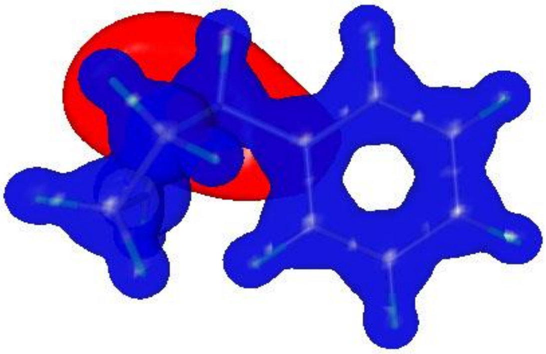

Figure 7. Isosurface representation of electrostatic potential of 2-phenyl-*3H*pyrrole molecule. Blue: positive potential (0.5 eÅ^{-3}), Red: negative potential (-0.5 eÅ^{-3}).

Table 3. Atomic Charges of 2-phenyl-*3H*pyrrole molecule.

Atom	NPA	MPA
C(1)	-0.051	-0.008
C(2)	-0.217	-0.038
C(3)	-0.222	-0.002
C(4)	-0.237	-0.045
C(5)	-0.220	0.007
C(6)	-0.230	-0.085
C(7)	-0.077	0.375
N(8)	-0.482	-0.567
C(8)	0.135	0.360
C(10)	-0.522	-0.020
C(11)	-0.463	0.024
H(12)	0.237	0.029
H(13)	0.235	0.016
C(14)	0.235	0.021
H(15)	0.235	0.017
H(16)	0.224	0.035
C(17)	0.237	-0.054
H(18)	0.206	-0.015
H(19)	0.234	-0.008
C(20)	0.259	0.007
H(21)	0.240	-0.042
H(22)	0.242	-0.008

Molecular electrostatic potential (MEP) generally present in the space around the molecule by the charge distribution is very useful in understanding the sites of electrophilic attacks and nucleopilic reaction for the study of charge transport process and hydrogen bonding interactions. In order to predict the molecular reactive sites, the MEP for our title molecule is calculated by B3LYP/aug-cc-PVDZ method as shown in Figure 7. The isosurface representation of ESP shows the large negative ESP surface is found near nitrogen atom, which indicates the negative charge domination of the molecule.

Conclusion

In summary, the quantum chemical, charge density and electronic and charge transport properties of OFETs based 2-phenyl-*3H*pyrrole molecule have been investigated through HF and DFT level of calculations. The optimized (B3LYP/aug-cc-PVDZ) geometric parameters are in excellent agreement with the experimental data. The dipole moment gives the very good information of conductivity. The HLG decreases from 12.08 to 5.504 eV. This variation is also confirmed from the spectrum of density of states (DOS), the significant decrease of HLG may facilitate large electron conduction through the 2-phenyl-*3H*pyrrole molecule. The MEP map shows that the negative potential sites are on electronegative atoms (nitrogen) while the positive potential sites are around the rest of molecule. These observations give an insight on this kind of structural and electronic properties, which are useful to design navel electronic devices. The atomic charges should be useful in molecular dynamics simulations. These observations give an insight on this kind of super conducting material, which are useful to design navel electronic devices.

References

[1]. S.C Lo, P.L. Burn, Chem. Rev. 107 (2007) 1097.
[2]. S. Chen, L. Deng, J. Xie, L. Peng, L. Xie, Q. Fan, W. Huang, Adv. Mater. 22 (2010) 5227.
[3]. J.E. Anthony, Chem. Rev. 106 (2006) 5028.
[4]. J. Zaumseil, H. Sirringhaus, Chem. Rev. 107 (2007) 1296.
[5]. J.E. Anthony, Angew. Chem., Int. Ed. 47 (2008) 452.
[6]. T.M. Clarke, J.R. Durrant, Chem. Rev. 110 (2010) 6736.
[7]. J.E. Allen, C.T. ACS Nano. 5 (2011) 7986.

[8]. D. E. Loy, B. E. Koene, M. E. Thompson, Adv. Funct. Mater. 12 (2002) 245.
[9]. C. W. Tang, S. A. Vanslyke, Appl. Phys. Lett. 51 (1987) 913.
[10].C. Adachi, K. Nagai, N. Tamoto Appl. Phys. Lett. 66 (1995) 2679.
[11].D. F. O'Brien, P. E. Burrows, S. R. Forrest, B. E. Koene, D. E. Loy, M. E. Thompson, Adv. Mater. 10 (1998) 1108.
[12].W. S. Hung, J. T. Lin, C. H. Chien, Y. T. Tao, S. S. Sun, Y. S. Wen, Chem. Mater. 16 (2014) 2480.
[13]. T. Otsubo, Y. Aso, F. Takimiya, J. Mater. Chem. 12 (2002) 2565.
[14]. Ping Li, Yahui Cui, Chongping Song, and Houyu Zhang, J. Phys. Chem. C 120 (2016) 14484.
[15].Narayanan Padma, Priya Maheshwari, D. Bhattacharya, B. Raj, Tokas, S. Sen, Y.Honda, S. Basu, P. K. Pujari, and T. V. Chandrasekhar Rao, ACS Appl. Mater. Interfaces. *8* (5) (2016) 3376
[16].K. Müllen, G. Wegner, *Electronic Materials: The Oligomer Approach*, Wiley-VCH, New York, NY, U.S.A. (1998).
[17]. R.Chang, J.H. Hsu, W.S. Fann, K.K. Liang, C.H. Chang, M. Hayahshi, J. Yu, S.H. Lin, E.C. Chang, K.R. Chuang, and S.A. Chen, Chem. Phys. Lett. 317 (2000) 142.
[18]. Y.T. Tao, E. Balasubramanian, A. Danel, B. Jarosz, and P. Tomasik, Chem. Mater. 13 (2001) 1207.
[20]. J.E. Anthony, Angew. Chem. Int. Ed. 47 (2008) 452.
[21]. R.F.W. Bader Atoms in Molecule: A Quantum Theory, Clarendon press, Oxford, UK (1990).
[22]. R.F.W. Bader, T.T. Nguyen-Dang, Adv Quantum Chem. 14 (1981) 63.
[23]. J.P. Perdew, Phys. Rev. B 33 (1986) 8822.
[24]. W. Kohn, L.J. Sham, Phys. Rev. 140 (1965) A1133.
[25]. A. Frish, E. Lecn, A.B.Nielson, A. Holder, A.J.Roy Dennigton, T.A. Keith, Gaussian Incorporated, Pittsburgh PA, (2003).
[26]. J. Cheeseman, T.A. Keith, R.F.W. Bader, AIMPAC Program Package, McMaster University Hamilton, Ontario, (1992).
[27]. AIMAll (Version 10.03.25) Todd A. Keith (aim.tkgristmill.com), (2010).
[28]. A. Volkov, P. Macchi, L.J. Farrugia, C. Gatti, P. Mallinson, T. Richter, T. Koritsanszky, XD2006 − a Computer Program for Multipole Refinement, Version 5.33. State University of New York at Buffalo, NY; Universita´ di Milano, Italy; University of Glasgow, UK; CNR-ISTM Milano, Italy; Free University of Berlin, Germany, (2007).
[29]. A. Stash, V. Tsirelson, J. Appl. Cryst, 35 (2002) 371.
[30]. A. Hagfeldt, M. Gratzel, Chem. Rev. 95 (1995) 49.
[31]. B. Parvanova and Galabov, J. Phys. Chem. A. 102 (1998) 1815.
[32]. Lu et al, J. Phys. Chem. A. 108 (2004) 4125.
[33]. J. Jang et.al, SID DIGEST. (2013) 1051.
[34]. T. Brinck, P. Jin, Y. Ma, J.S. Murray, P. Politzer, J. Mol. Model 9 (2003) 77.
[35]. R.S. Mulliken, J. Chem. Phys. 23 (1955) 1833.
[36]. A.E. Reed, L.A. Curtiss, F. Weinhold, Chem. Rev. 88 (1988) 899.